Catalysis Today 155 (2010) 123–130

Contents lists available at ScienceDirect

Catalysis Today

journal homepage: www.elsevier.com/locate/cattod

Flame dynamics in catalytic and non-catalytic mesoscale microreactors

Gianmarco Pizza[a,b], John Mantzaras[a,*], Christos E. Frouzakis[b]

[a] Paul Scherrer Institute, Combustion Research, CH-5232, Villigen PSI, Switzerland
[b] Aerothermochemistry and Combustion Systems Laboratory, Swiss Federal Institute of Technology, CH-8092, Zurich, Switzerland

ARTICLE INFO

Keywords:
Flame dynamics in mesoscale combustion
Combustion instabilities
Catalytic combustion
Platinum catalyst
Spectral element method

ABSTRACT

The dynamics of fuel-lean (equivalence ratio $\varphi = 0.5$) premixed hydrogen/air flames are investigated numerically in a 2-mm-height planar channel with platinum-coated walls, as a function of the inlet velocity and catalytic reactivity. An elliptic 2-D transient code is used, with elementary heterogeneous (catalytic) and homogeneous (gas-phase) chemical reaction schemes and detailed transport. The channel wall temperature is prescribed and the inlet properties are uniform. The catalytic reactivity is controlled by varying the model parameter A_s, which denotes the ratio of the catalytically active area to the geometrical channel surface area. It is shown that the rich flame dynamics of the non-catalytic case ($A_s = 0$), which include non-stationary repetitive ignition/extinction and oscillating flames, can be suppressed by suitable selection of the catalytic reactivity. The repetitive/ignition extinction flames are eliminated at $A_s = 0.003$ and the oscillating ones for $A_s > 0.01$, while for higher values of A_s only stationary "closed symmetric" and "asymmetric" flames are obtained. The results suggest that the application of a predetermined catalyst loading on the channel walls is a feasible method to eliminate unsteady combustion modes in practical mesoscale reactors.

1. Introduction

Mesoscale combustion applications range from portable power/heat generation [1–4] to larger scale industrial applications (e.g. burners for reheat stages of gas turbines, reactors that provide heat for steam reforming units, etc.). The term "mesoscale" refers to burners with sizes of the order of the quenching distance. In such combustors, in addition to the instabilities of a freely propagating flame (which are hydrodynamic and thermal-diffusive in nature), a flame also experiences developing boundary layers, heat transfer to and from the walls, radical quenching and/or surface reactivity, which in turn add to the complexity of the system. The non-linear interaction between these effects gives rise to a wealth of combustion dynamics. Experimental and numerical work in the literature has reported different combustion modes for flames in mesoscale non-catalytic channels.

In the experiments of Dogwiler et al. [5], asymmetric flames were observed in fuel-lean ($\varphi = 0.33$) methane/air mixtures burning in a rectangular channel with a height of 7 mm; the sensitivity of the asymmetric flame to small experimental perturbations resulted in a temporally random transition between an upper and a lower asymmetric flame structure. Maruta et al. [6] studied experimentally the characteristics of methane/air and propane/air premixed flames in cylindrical tubes of 2 mm inner diameter with a fixed wall temperature profile. They observed stationary flames, cyclic oscillatory flames, and repetitive ignition and extinction, at different values of the inflow velocity. The repetitive extinction/ignition combustion mode was also observed in the nonpremixed methane/oxygen flame experiments of Richecoeur and Kyritsis [7] inside a 4 mm diameter curved duct. Pizza et al. [8] have investigated numerically the stabilization and dynamics of lean premixed hydrogen/air flames in planar non-catalytic channels with heights (h) ranging between 0.3 and 1.0 mm (these sizes are smaller than the mesoscale range and are usually referred to as microscale), aspect ratio 1:10, and inflow velocities covering the full range of flame stabilization within the channel. The results have shown the existence of stationary symmetric and asymmetric flames as well as non-stationary flames for the wider channels ($h > 0.8$ mm). These findings suggested that richer and even more complex flame dynamics maybe expected at even larger channel heights, i.e. at the mesoscale range. Indeed, simulations in mesoscale ($2 \leq h \leq 7$ mm) channels with inert walls, revealed six different burning modes (mild combustion, ignition/extinction, closed steady symmetric flames, open steady symmetric flames, oscillating, and asymmetric flames) [9]. Kurdyumov et al. studied both experimentally [10] and numerically [11] the dynamics of premixed methane/air flames in a 21.4 mm inner diameter tube at conditions close to the flashback limit, showing that for certain

* Corresponding author. Tel.: +41 56 3104046; fax: +41 56 3102199.
E-mail address: ioannis.mantzaras@psi.ch (J. Mantzaras).

0920-5861/$ – see front matter © 2010 Elsevier B.V. All rights reserved.
doi:10.1016/j.cattod.2010.04.029

sets of parameters, the flame exhibits coexistence of steady and oscillatory states.

The experimentally and numerically observed unsteady combustion modes may compromise the integrity and safe operation of burners. Pizza et al. [12] analyzed the effectiveness of catalytic reactions on the suppression of the flame dynamics observed in a microscale channel (h = 1 mm) [8]. It was found that all unsteady and asymmetric flame modes could be effectively suppressed by coating the channel walls with platinum.

In the present work, the dynamics of fuel-lean (φ = 0.5) hydrogen/air flames in catalytic (Pt-coated) and non-catalytic planar channels with a height of 2 mm and a length of 20 mm, are investigated numerically by means of transient direct numerical simulations (DNS) with detailed hetero-/homogeneous chemistry and transport. The main objective is to identify the gas-phase combustion dynamics at this mesoscale channel size and to assess the impact of catalytic reactions on the dynamics. The resulting flame modes are mapped as a function of two parameters: the inflow velocity, U_{IN}, and the catalytic reactivity, A_{s}. The latter is controlled by the ratio of the active-to-geometrical surface area. Implications for the suppression of combustion dynamics for reactor design are finally drawn.

2. Computational approach

The configuration consists of a channel flow established between two parallel, infinitely wide plates, with a length L = 20 mm and a height h = 2 mm. Details of the numerical method for the non-catalytic channels can be found in Ref. [8]. The model is briefly described next, emphasizing the treatment of surface reactions.

2.1. Numerical model

The numerical code solves the transient 2-D continuity, momentum, energy, and gas-phase species equations for ideal reactive gases at the low Mach number limit. To account for catalytic chemistry, the surface species coverage (θ_k) equations are also solved [13]:

$$\frac{\partial \theta_k}{\partial t} = \frac{\dot{s}_k}{\Gamma}, \quad k = 1, \ldots, N_{\mathrm{s}}, \tag{1}$$

with Γ the surface site density of the catalyst, $\dot{s}_k$ the catalytic molar production rate of the kth surface species and N_{s} the number of surface species.

At the gas–solid interface, the species boundary conditions read:

$$\vec{n} \cdot \left[\rho Y_i \left(\vec{V}_i + \vec{u}\right)\right]_{\mathrm{wall}} = A_{\mathrm{s}} \dot{s}_i W_i, \quad i = 1, \ldots, N_{\mathrm{g}}, \tag{2}$$

where ρ is the gas density, Y_i, $\vec{V}_i$, W_i and $\dot{s}_i$ are the mass fraction, diffusion velocity vector, molecular weight, and molar catalytic production rate of the ith gas-phase species, respectively; N_{g} is the number of gaseous species; $\vec{n}$ is the unit outward-pointing vector normal to the surface, and $\vec{u}$ is the Stefan velocity given by $\vec{n} \cdot \vec{u} = (1/\rho)\sum_{i=1}^{N_{\mathrm{g}}} A_{\mathrm{s}} \dot{S}_i W_i$ [13]. The ratio of the catalytically active area to the geometrical channel area, A_{s}, is a crucial parameter in the modeling of reactors coated with technical catalysts and can be assessed in practice via CO or H_2 chemisorption experiments [14,15].

A fuel-lean (φ = 0.5), hydrogen/air premixture is fed at the channel inlet at atmospheric pressure. Uniform inlet velocity (U_{IN}), flux boundary conditions for the incoming species mass fractions and constant inlet temperature (T_{IN} = 300 K) are specified at the inflow. Along the catalytic walls, the temperature is prescribed (ramping smoothly over the initial 1 mm channel length via a hyperbolic tangent function from the incoming mixture temperature, T_{IN} = 300 K, to the final value T_{W} = 960 K), while no-slip is imposed for the axial velocity. The selected wall temperature should be tolerable by materials used for microreactors. A wide variety of steels (class 400) commonly used for reactor construction have maximum operational temperatures around 960 K (for example, steel 410: 980 K, steel 416: 950 K, and steel 420: 895 K). Higher wall temperatures (up to 1400 K) can be tolerated by ceramic materials. However, at such temperatures the high reactivity of hydrogen leads to flames anchored close to the entry and unrealistically high velocities (U_{IN} > 150 m/s) are required to shift the anchoring point downstream. At the outlet, zero-Neumann boundary conditions are imposed for all variables. For the examined ranges of U_{IN}, the flow is laminar with inlet Reynolds number ranging from 0.5 to 212. Finally, buoyancy is neglected.

For gas-phase chemistry, the elementary mechanism of Kim et al. [16] with 9 species and 21 reactions is employed. The detailed surface reaction scheme of Deutschmann et al. [17] (6 gaseous species, 5 surface species and 14 reactions) describes the oxidation of hydrogen on platinum with a surface site density $\Gamma = 2.7 \times 10^{-9}$ mol/cm^2. A mixture-average transport model is adopted for the species diffusion velocity, using the CHEMKIN transport database [18], and the gas-phase and surface reaction rates are evaluated with CHEMKIN [19] and Surface CHEMKIN [13], respectively.

The parallel code employs the spectral element method for the spatial discretization. The computational domain is split into quadrilateral conforming elements; within each element, Nth order polynomials are used to interpolate the solution in each spatial direction [20]. Time integration is performed with a high-order splitting scheme for low Mach number reactive flows [21], whereby the continuity and momentum equations are integrated with a semi-implicit scheme and the species and energy equations are integrated implicitly using CVODE [22].

2.2. Computational domain

The entire 2-D channel domain (symmetry is not invoked as to allow for asymmetric flame structures) is discretized with 8 spectral elements in the transverse direction and 60 elements in the streamwise direction, all equally spaced. The resolution requirements are determined based on the thermal flame thickness, L_{f}, [23]: $L_{\mathrm{f}} = (T_{\mathrm{f}} - T_{\mathrm{IN}})/\max\left|\partial T/\partial x\right|$, with T_{IN} and T_{f} the temperatures of the fresh and burned mixture, respectively, and $\max\left|\partial T/\partial x\right|$ the maximum temperature gradient along the flame coordinate. Using the PREMIX code of CHEMKIN [24], the flame thickness and laminar flame speed of a 1-D freely propagating lean premixed laminar H_2/air flame (φ = 0.5, T_{IN} = 300 K) are found to be L_{f} = 0.39 mm and S_{L} = 58 cm/s, respectively.

Employing eight-order Legendre–Lagrangian interpolating polynomials per direction and element, a total of 481 axial grid points are used, corresponding to an average spatial resolution of Δx = 0.042 mm and resulting in approximately $L_{\mathrm{f}}/\Delta x$ = 9 grid points within the flame. The results were not significantly affected by increasing the polynomial order to 10 and subsequently to 12, corresponding to 12 and 14 points inside the flame, respectively, confirming the grid-independence of the solution. Since the grid is even finer in the transverse (y) direction, further y-resolution tests were not necessary. Simulations were performed on a Linux cluster with 2.4 GHz CPUs. The stiffness of the surface reactions in Eqs. (1) and (2) resulted in high computational cost: for a grid consisting of a total of 30,784 discretization points, up to 200 h were necessary on 8 CPUs to obtain the final state (steady or oscillatory) for some of the points in the forthcoming Fig. 1. It is worth pointing out that full 2-D transient simulations (i.e. without invoking the quasi-steady state assumption for the surface species) have not yet been reported in mesoscale channels with detailed hetero-/homogeneous reaction schemes.

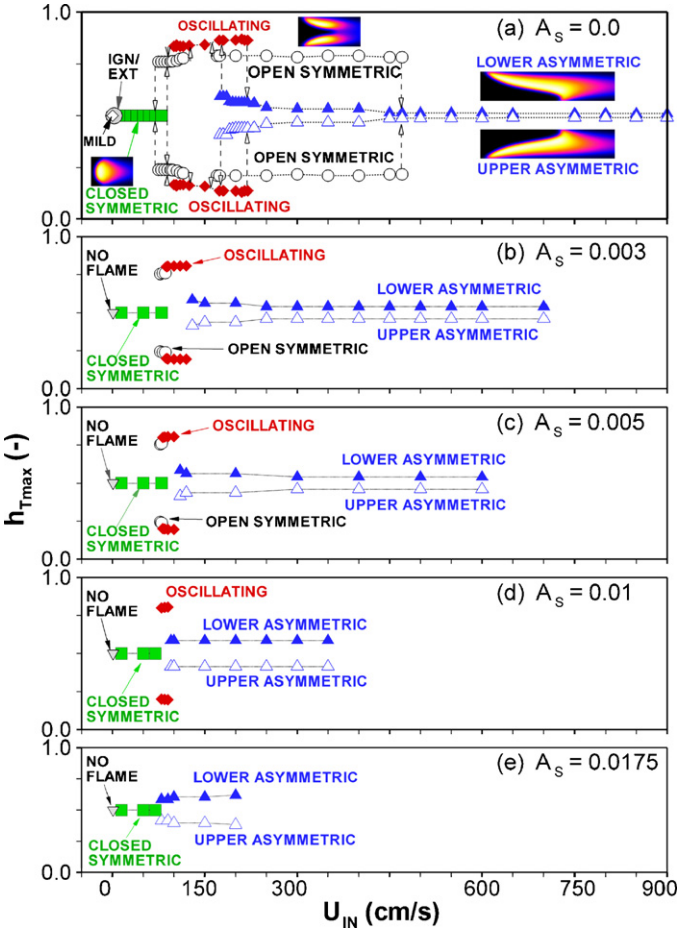

Fig. 1. Combustion mode types and range of inflow velocity over which they are observed for different surface reactivities A_s. The vertical axis h_{Tmax} denotes the transverse distance from the lower channel wall ($y = 0$) of the point of the maximum temperature, normalized by the channel height h. For symmetric combustion modes $h_{Tmax} = 0.5$, while for asymmetric flames h_{Tmax} is either smaller or greater than 0.5. The dashed vertical lines with the hollow arrow indicate the transitions in the combustion modes observed upon variation of U_{IN}. The images in (a) provide the flame shapes of different combustion modes via the Y_{OH} distributions at the vicinity of the flame (color online).

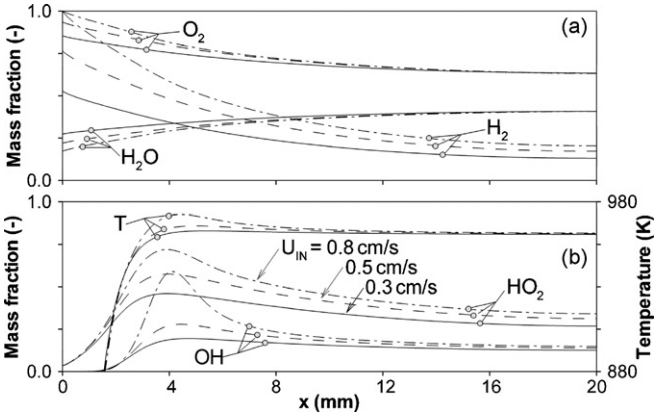

Fig. 2. Mild combustion at $U_{IN} = 0.3$ cm/s (solid lines), 0.5 cm/s (dashed lines), and 0.8 cm/s (dashed–dotted lines) for $A_s = 0.0$: species mass fractions ($217.4 \times Y_{H_2}$, $5.26 \times Y_{O_2}$, $3.33 \times Y_{H_2O}$, $5.0 \times 10^5 \times Y_{OH}$, $7.69 \times 10^3 \times Y_{HO_2}$) and temperature along the channel midplane.

3. Results and discussion

The results for the non-catalytic cases ($A_s = 0$) are first reviewed and then the impact of increasing surface reactivity on the flame dynamics is examined.

3.1. Non-catalytic channels

Detailed description of the flame dynamics for the non-catalytic case ($A_s = 0$) is provided in Ref. [9]; in the present work an overview of the combustion modes is presented with emphasis on some peculiarities not reported previously. The observed flame types are summarized in Fig. 1(a) as a function of the inflow velocity. To facilitate the graphical presentation of all flame solutions, the parameter h_{Tmax} has been defined: it denotes the transverse distance from the lower channel wall ($y = 0$) to the point of the maximum temperature, normalized by the channel height h. The modes shown in Fig. 1(a) include mild combustion (open diamond), repetitive ignition/extinction (filled circles), closed steady symmetric flames (open squares), open steady symmetric flames (open circles), oscillating flames (filled diamonds), and steady asymmetric flames (open and filled triangles for the upper and lower asymmetric flames, respectively). For the mild combustion, ignition/extinction mode and closed flames, the maximum temperature is located at the midplane, such that $h_{Tmax} = 0.5$. For the asymmetric flames the maximum is away from the midplane and h_{Tmax} is either smaller or greater than 0.5; for the oscillating flame, h_{Tmax} continuously varies in time between the two limiting values marked with filled diamonds in Fig. 1(a); finally, for the open flame the two open circles at a given value of U_{IN} represent the location of the maximum temperature in the two separate branches of this flame, as will be elaborated next. The vertical dashed lines with hollow arrows in Fig. 1(a) indicate the transitions between the different flame types as they were observed by varying the inflow velocity.

The mild combustion mode [6,25], observed for the lowest inflow velocities considered herein ($0.3 \le U_{IN} \le 0.8$ cm/s), is presented in Fig. 2: the change in the species axial profiles along the channel midplane is gradual (there are no localized peaks typical of vigorous combustion) and the maximum temperature increase above the wall temperature of 960 K due to combustion is only 3, 6, and 13 K for $U_{IN} = 0.3$, 0.5, and 0.8 cm/s, respectively. Hydrogen is being consumed over the entire channel length, resulting in a total conversion of 75%, 77%, and 80% at the channel exit for $U_{IN} = 0.3$, 0.5, and 0.8 cm/s, respectively. The rising hydrogen conversion with increasing U_{IN} is an outcome of the species flux inlet boundary condition; at such low velocities, it results in different hydrogen mass fractions at $x = 0$ (see Fig. 2(a)).

The ignition/extinction mode ($0.9 \le U_{IN} \le 5.0$ cm/s) is illustrated in Fig. 3 for $U_{IN} = 5$ cm/s. Fig. 3(a) shows the time history of the heat release rate integrated over the entire domain (HRR), non-dimensionalized by the reference temperature $T_{ref} = T_{IN} = 300$ K, the reference heat capacity of the incoming mixture $c_{p,ref} = 1.2007$ kJ/(kg K) and the reference time $t_{ref} = h/U_{IN}$. The flame is characterized by a periodic repetition (33 Hz at $U_{IN} = 5$ cm/s) of ignition (as seen in Fig. 3(c) and (f) presenting 2-D maps of Y_{OH} and Y_{H2} at time t_1), subsequent flame propagation (Fig. 3(d) and (g), time t_2) and finally extinction close to the channel inlet (Fig. 3(e) and (h), time t_3). Ignition is characterized by the formation of two initial circular kernels close to the hot walls (Fig. 3(c) and (f)), which expand until they approach each other in the middle of the channel; from then on, the flame can only propagate horizontally (Fig. 3(d) and (g)), both upstream and downstream. The formation of two ignition kernels is a new feature not reported in Ref. [9] and it is linked to the particular inflow velocity; at low U_{IN} only single ignition kernels are formed. The upstream propagating front extinguishes at about $x = 1.2$ mm due to heat losses to the cold inflow, and the downstream propagating one at about $x = 16.5$ mm, whereby the local hydrogen mass fraction drops below

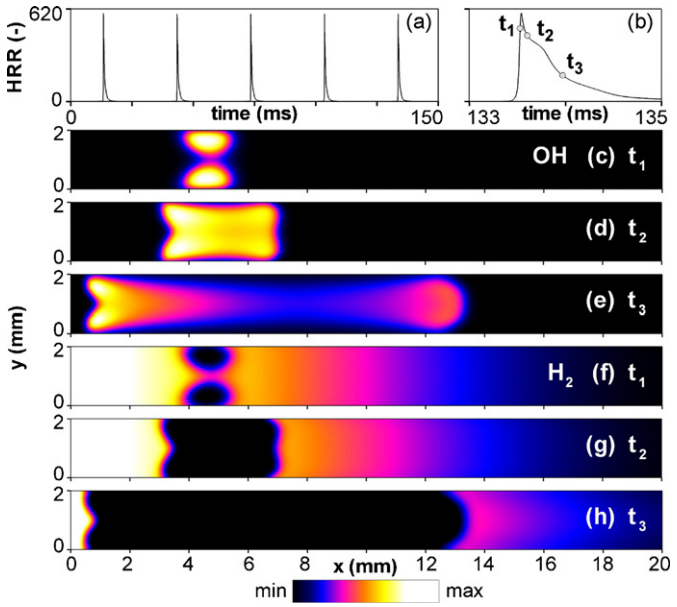

Fig. 3. Ignition/extinction mode at U_{IN} = 5.0 cm/s for A_s = 0.0: (a) temporal variation of the integrated heat release rate inside the channel; (b) expanded detail of (a); (c–e) and (f–h) 2-D maps of the Y_{OH} and Y_{H_2}, respectively, at the three times t_1–t_3 marked in (b) (t_1 = 133.53 ms, t_2 = 133.6 ms, and t_3 = 133.97 ms). The minimum in the color coded bar corresponds to zero for Y_{OH} and Y_{H_2}, while the maximum to $Y_{OH} = 5.4 \times 10^{-3}$, 6.2×10^{-3}, and 5.0×10^{-3}, in (c–e), respectively, and to 1.2×10^{-2} for Y_{H_2} (color online).

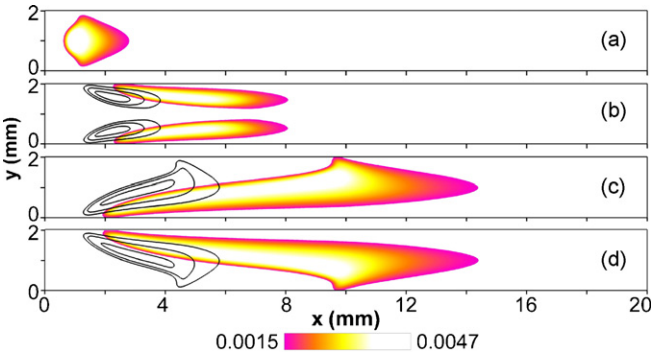

Fig. 4. OH mass fraction color iso-contours ($0.0015 \le Y_{OH} \le 0.0047$) and three iso-lines (in the range $0.0016 \le Y_{OH} \le 0.0035$ in (b) and $0.002 \le Y_{OH} \le 0.0039$ in (c, d)) for A_s = 0.0: (a) closed symmetric flame at U_{IN} = 95 cm/s; (b) open symmetric flame; (c) upper asymmetric flame; (d) lower asymmetric flame. In (b–d) U_{IN} = 200 and 450 cm/s for the iso-lines and iso-contours, respectively (color online).

the lean flammability limit (Fig. 3(e) and (h)). During this process, both fronts change their curvature from initially convex to concave towards the fresh mixture. The fuel conversion is incomplete, and the mass fraction of molecular hydrogen at the channel exit varies in time between the values 1.03×10^{-3} and 2.05×10^{-3} within one period of the mode.

In Fig. 4, 2-D maps of Y_{OH} are shown for: (a) the steady closed symmetric flames ($4 \le U_{IN} \le 95$ cm/s), (b) the steady open symmetric flames ($75 \le U_{IN} \le 115$ cm/s and $170 \le U_{IN} \le 470$ cm/s), and (c, d) the steady asymmetric flames ($174 \le U_{IN} \le 900$ cm/s). In Fig. 4(b–d) three iso-lines and iso-contours of Y_{OH} are superimposed at two different inlet velocities. An increase of the

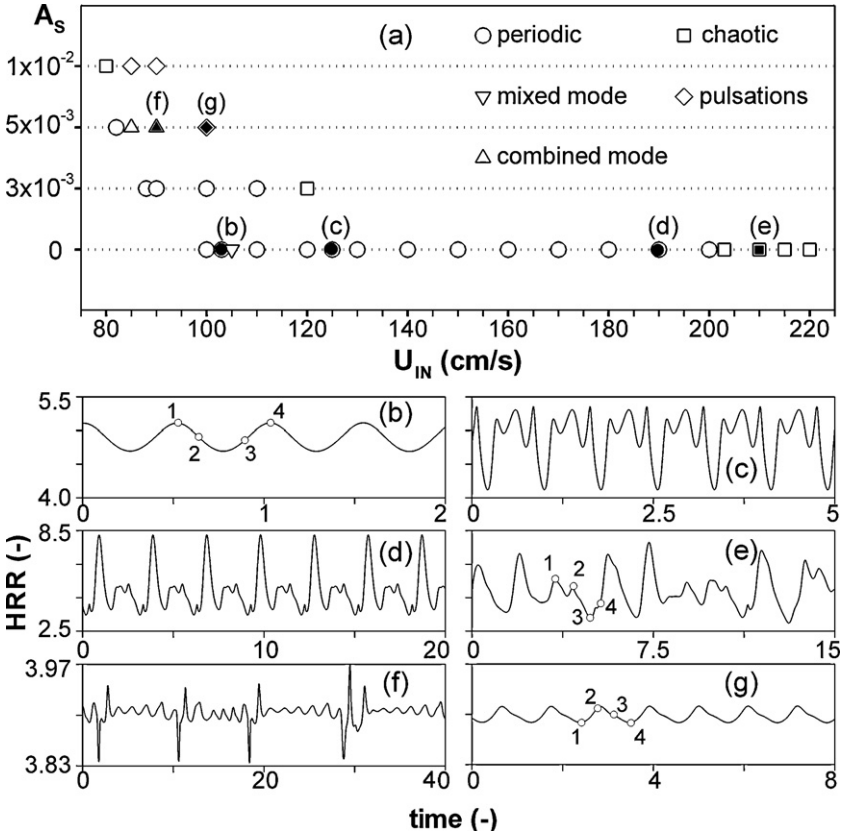

Fig. 5. Map of oscillating flames for various U_{IN} and A_s (a). Plates (b–g) provide the temporal evolution of the integrated heat release rate (HRR). For A_s = 0.0: periodic oscillations at U_{IN} = 103.5, 125 and 190 cm/s in (b–d), respectively; (e) chaotic oscillation at U_{IN} = 210 cm/s. For A_s = 0.005: (f) combined mode oscillation at U_{IN} = 90 cm/s and (g) pulsating flame at U_{IN} = 100 cm/s. The locations in A_s–U_{IN} space of plates (b–g) are marked with filled symbols in plate (a).

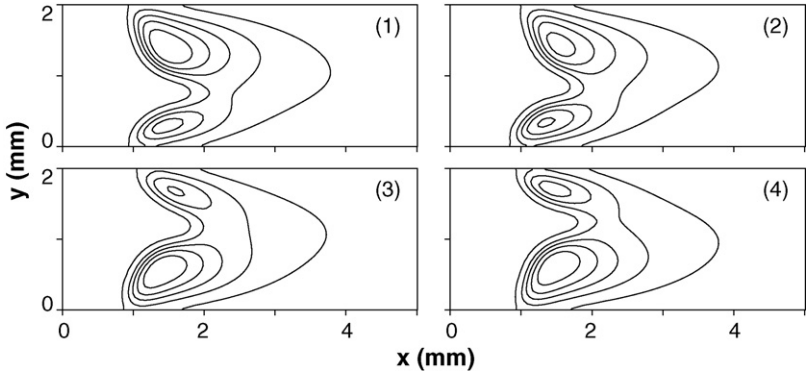

Fig. 6. Oscillating flame at U_{IN} = 103.5 cm/s for A_s = 0.0: five Y_{OH} iso-lines (ranging from $0.0006 \le Y_{OH} \le 0.0034$) at the four instants marked in Fig. 5(b).

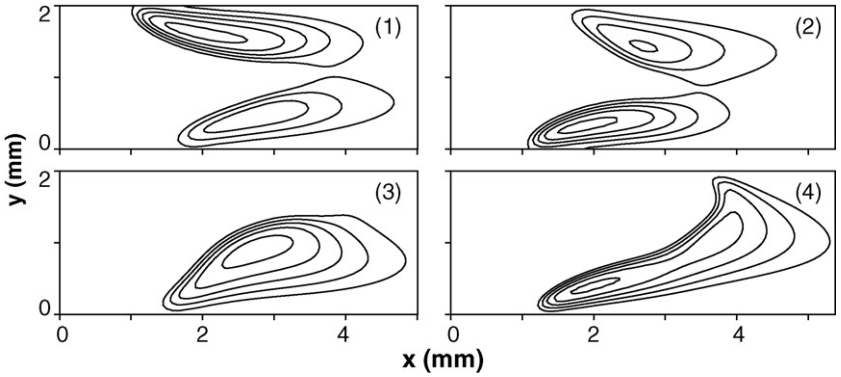

Fig. 7. Oscillating flame at U_{IN} = 210 cm/s for A_s = 0.0: five Y_{OH} iso-lines (ranging from $0.0014 \le Y_{OH} \le 0.0046$ in (1, 2), from $0.0014 \le Y_{OH} \le 0.0041$ in (3), and from $0.00185 \le Y_{OH} \le 0.0039$ in (4)) at the four instants marked in Fig. 5(e).

inlet velocity from 200 to 450 cm/s elongates significantly both the open and asymmetric flames but has a smaller impact on the flame anchoring position. For all the aforementioned steady flame types, complete fuel conversion is attained at the channel exit.

For the oscillating flames, Fig. 5 provides the time history of HRR at increasing U_{IN} and for selected values of A_s. The lowest series of data points in Fig. 5(a) represents the oscillating flames in the non-catalytic channel (A_s = 0). For $100 \le U_{IN} \le 200$ cm/s the oscillations are periodic: at U_{IN} = 103.5 cm/s, for example, a harmonic (single frequency) evolution of HRR is observed (Fig. 5(b)), whereas at higher U_{IN} more complex periodic behavior appears (Fig. 5(c) and (d)). Chaotic oscillations appear in the range $200 \le U_{IN} \le 220$ cm/s, see Fig. 5(e) for U_{IN} = 210 cm/s. The time evolution of the flame structure for the oscillating flames at U_{IN} = 103.5 and 210 cm/s is described with the aid of the Y_{OH} iso-lines in Figs. 6 and 7, respectively. The harmonic oscillation, U_{IN} = 103.5 cm/s in Fig. 6, is characterized by two flame branches which periodically and alternately expand and contract, with the maximum HRR reached when either branch attains its maximum size. Therefore, the oscillation period is twice the one deduced from Fig. 5(b). The minimum HRR, on the other hand, is reached when the two branches are of equal size. At U_{IN} = 105 cm/s, the harmonic oscillations are interrupted at random time intervals by the temporary merging of the two flame branches (this combustion mode is referred to as mixed mode [9]). The chaotic oscillations are characterized (see Fig. 7 for U_{IN} = 210 cm/s) by the two flame branches expanding and contracting such that at some instants only one branch is left while the other one completely extinguishes (Fig. 7(3)) but re-emerges later on (Fig. 7(4)) and starts to grow at the expense of the other branch. For all oscillating flames, the fuel is fully consumed at the channel exit.

3.2. Flame dynamics in the presence of catalytic reactions

In order to study the influence of catalytic activity on the flame dynamics, the surface reactivity is gradually increased by adjusting the surface area ratio A_s in Eqs. (2). In technical systems with a well-dispersed catalyst, A_s is larger than unity such that the catalytic conversion rates of the typically less reactive hydrocarbon fuels are enhanced. However, because of the very high reactivity of hydrogen on platinum, a mass-transport-limited catalytic conversion is already achieved at A_s = 1. Therefore, the effects of finite-rate surface chemistry on the flame dynamics were investigated by reducing A_s to suitably low values ($3.0 \times 10^{-3} \le A_s \le 1.75 \times 10^{-2}$). Such values can be realized in practice by a very low loading of Pt on the catalyst washcoat.

The axial profiles of $Y_{H_2,mid}$, the hydrogen mass fraction at the channel midplane (y = 1.0 mm), normalized by $Y_{H_2,IN}$, are plotted in Fig. 8 for the case of pure catalytic reactions (no gas-phase chemistry included) at four different A_s. Even at such low values of A_s,

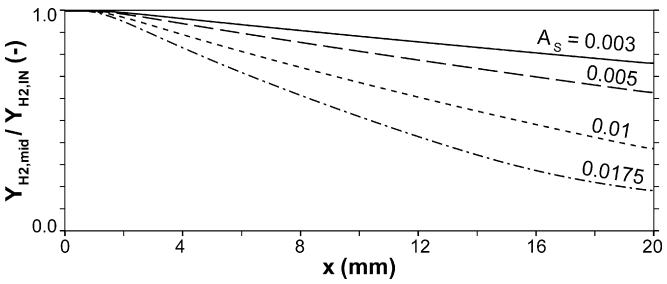

Fig. 8. Hydrogen mass fraction along the channel midplane, $Y_{H_2,mid}$, normalized by the inlet value $Y_{H_2,IN}$: pure catalytic conversion for U_{IN} = 100 cm/s at different A_s.

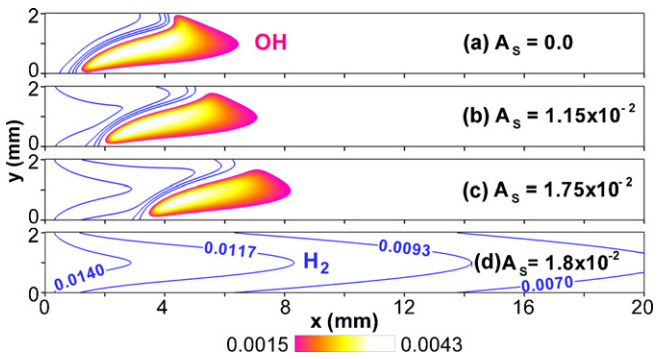

Fig. 9. Iso-contours of OH mass fraction ($0.0015 \le Y_{OH} \le 0.0043$) and four iso-lines of Y_{H_2} (ranging from 0.014 to 0.007) at $U_{IN} = 200$ cm/s for different surface reactivities A_s: (a) pure gas-phase combustion ($A_s = 0.0$); (b) $A_s = 1.15 \times 10^{-2}$; (c) $A_s = 1.75 \times 10^{-2}$; (d) $A_s = 1.8 \times 10^{-2}$. In (d) the fuel conversion is pure heterogeneous (the maximum of Y_{OH} is 1.433×10^{-8}) (color online).

the catalytic fuel depletion is noticeable. It will be shown next that such modest catalytic reactivities are sufficient to drastically alter the underlying flame dynamics.

The effect of catalytic reactivity on the asymmetric flames is analyzed first. Fig. 9 illustrates the changes of the flame structure of the originally asymmetric flame at $U_{IN} = 200$ cm/s and $A_s = 0$. As A_s increases, the flame first shifts downstream due to the catalytic depletion of hydrogen and at the same time its degree of asymmetry decreases (Fig. 9(b) and (c)). Eventually, the flame extinguishes at $A_s = 1.8 \times 10^{-2}$ (Fig. 9(d)) leading to pure heterogeneous conversion of hydrogen. It is hence not possible to restore full symmetry in the asymmetric flames by increasing A_s, as was the case at the microscale ($h = 1$ mm) channels [12].

The impact of surface reactions on the oscillating flames is presented in Fig. 5. An increase of A_s has two effects. First, the range of inflow velocities over which oscillating flames are obtained becomes narrower (Fig. 5(a)). In addition, the oscillations qualitatively change, and two new modes (the pulsating and the combined mode) arise. At $A_s = 0.003$ periodic and chaotic oscillations survive, however over a much narrower range of inflow velocities. At $A_s = 0.005$ and for the lowest values of U_{IN} (i.e. close to the lower limit of the stability range of oscillating flames), periodic oscillations (marked with a circle in Fig. 5(a)) qualitatively similar to the ones of the non-catalytic channel presented in Fig. 5(b) and Fig. 6 are observed. When the inflow velocity approaches the upper limit of the stability range, pulsating flames (marked with diamonds in Fig. 5(a)) similar to the ones reported in Ref. [8] are observed. Fig. 10 provides the Y_{OH} iso-lines (a–d) and the surface coverage (e–h) at the four time instants marked on the HRR curve in Fig. 5(g) for the pulsating flame ($A_s = 0.005$ and $U_{IN} = 100$ cm/s): one of the two flame anchoring points (either on the lower or on the upper wall) remains practically fixed while the other one moves back and forth in the streamwise direction in a periodic manner (Fig. 10). Both cases, with either the lower anchoring point fixed and the upper one moving (shown in Fig. 10) or the opposite, were observed in the simulations. At intermediate values of U_{IN} a combination of the harmonic oscillation and the pulsation is observed, giving rise to a new oscillatory mode which will be referred to as the combined mode. For this mode, the temporal evolution of the flame shape is such that during certain periods the flame oscillates as in Fig. 6 (i.e. with two separate branches alternatively expanding and contracting), while during other periods it pulsates like the flame of Fig. 10. The surface coverage in Fig. 10 indicates a light-off zone extending over about 0.5 mm (wherein the H(s) drops sharply); this is due to the imposed wall temperature ramp described in Section 2.1. Fol-

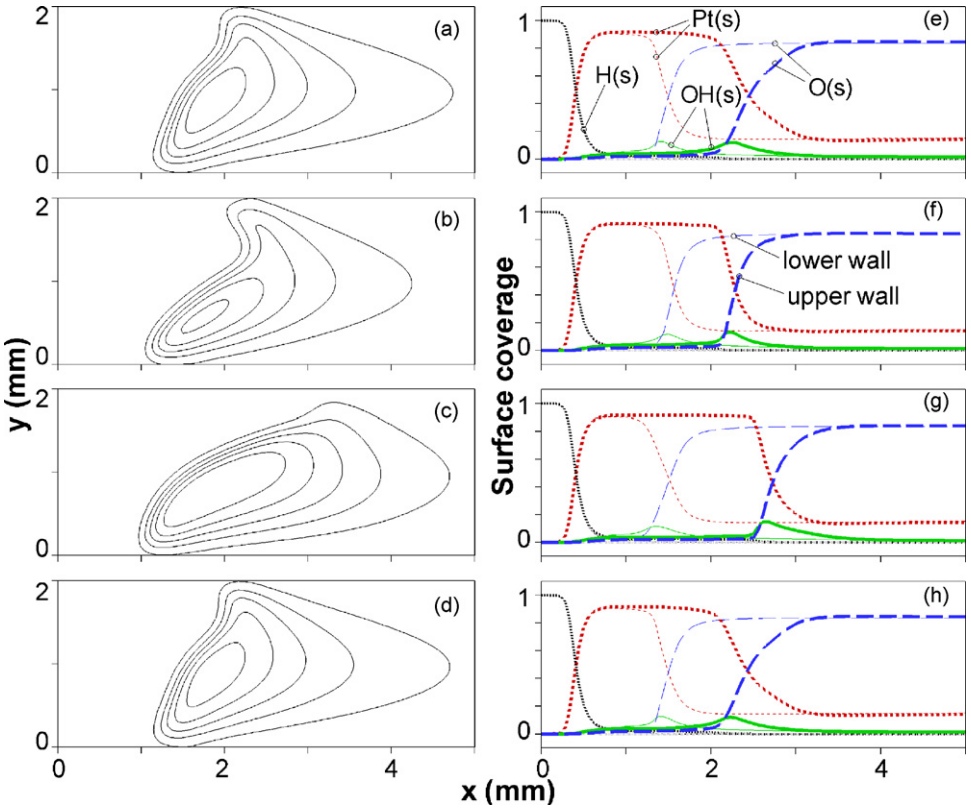

Fig. 10. Pulsating flame at $U_{IN} = 100$ cm/s for $A_s = 5.0 \times 10^{-3}$: (a–d) five Y_{OH} iso-lines (in the range $0.0007 \le Y_{OH} \le 0.0034$) at the four time instants marked in Fig. 5(g); (e–h) the corresponding surface coverage on the lower (thin lines) and upper (thick lines) channel wall. The H(s) coverage for both upper and lower walls practically coincide (color online).

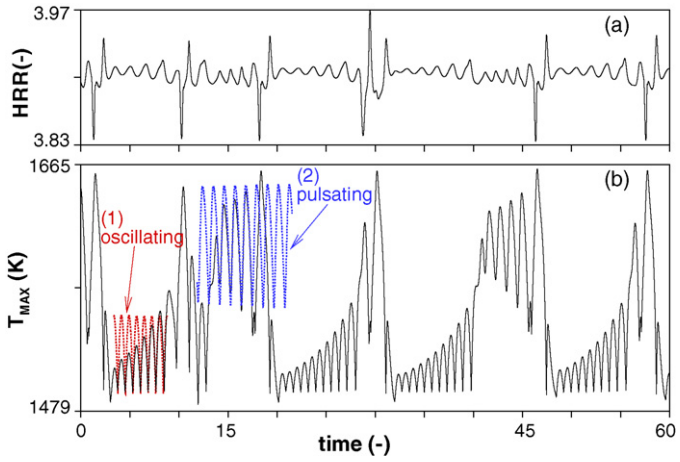

Fig. 11. Combined mode at U_{IN} = 90 cm/s for $A_s = 5.0 \times 10^{-3}$: time evolution of (a) heat release rate HRR and (b) maximum temperature T_{MAX}. For the same value of A_s, in (b) the T_{MAX} signals for the oscillating flame at U_{IN} = 82 cm/s, and (2) the pulsating flame at U_{IN} = 100 cm/s, are superimposed. The signal in Fig. 5(f) is an enlargement of (a) (color online).

lowing light-off, Pt(s) and O(s) constitute the main coverage before and after the flame, respectively.

Fig. 11 shows the temporal evolution of the HRR and the maximum temperature T_{MAX} for the combined mode of oscillation at U_{IN} = 90 cm/s and A_s = 0.005. In Fig. 11(b), the maximum temperature for the harmonically oscillating flame (U_{IN} = 82 cm/s and A_s = 0.005) and the pulsating flame (U_{IN} = 100 cm/s and A_s = 0.005) are superimposed to the T_{MAX} curve of the combined mode. During the time interval of the oscillating flame, the oscillations of the combined mode are harmonic but of increasing amplitude. The maximum alternate expansion of the two flame branches keeps increasing until eventually one of them completely disappears. Subsequently, only one burning branch extending asymmetrically between the two walls is formed and starts to oscillate in a fashion similar to the pulsating flame. The pulsation amplitude is again growing in time, until the flame breaks up in the middle and the harmonically oscillating flame is established again. This continuous transition between the two modes appears at random time instants.

For four chosen values of the surface reactivity (A_s = 0.003, 0.005, 0.01, and 0.0175), the inflow velocity was varied systematically in order to cover all possible flame positions within the computational domain. The results are presented in Fig. 1(b–e) for increasing A_s. For all investigated values of the surface reactivity, the mild and the repetitive ignition/extinction modes are completely suppressed. The reason is that at the low inlet velocities (long residence times) of these modes, the heterogeneous pathway is very effective in consuming hydrogen, depriving the gas-phase from fuel and hence inhibiting homogeneous ignition. Therefore, at the lowest values of the inflow velocity, only flameless, pure heterogeneous conversion is observed. This new combustion mode, marked in Fig. 1(b–d) with a triangle, is denoted by "no flame".

For A_s = 0.003, Fig. 1(b), the dynamics have already changed considerably compared to pure homogeneous combustion in Fig. 1(a): the mild and the ignition/extinction modes have been suppressed; the stability ranges of oscillating (see also Fig. 5(a)) and of open symmetric flames have been considerably reduced; and the U_{IN} at which the downstream anchoring point of the asymmetric flame reaches the outflow section is reduced from 900 to 700 cm/s. For A_s = 0.005 and 0.01, Fig. 1(c) and (d), the stability range of oscillating, open symmetric, and asymmetric flames shrinks even further, whereas the combined mode and pulsating flames appear. By increasing A_s to the highest value considered in this study (A_s = 0.0175), all the oscillating modes are completely suppressed and only stationary closed symmetric and asymmetric flames are left (Fig. 1(e)). It is nonetheless obvious that, with increasing surface reactivity, the maximum value of U_{IN} for which flames can be sustained inside the channel is considerably reduced: $U_{IN,max}$ = 900 and 200 cm/s for A_s = 0.0 and 0.0175, respectively; see Fig. 1(a) and (e).

The suppression of all non-stationary flame modes (ignition/extinction, oscillating and pulsating) is desirable as these may compromise the reactor performance and integrity. Therefore, the catalytic coating of the channel walls provides a very effective method for eliminating all non-stationary combustion modes. Depending on the fuel, catalyst and geometry, an analysis similar to the one presented here can provide the minimum catalytic reactivity (A_s) needed to suppress undesired flame dynamics while still maintaining predominantly gas-phase combustion. A catalyst with a predetermined noble-metal loading can then be applied at the channel walls so as to reproduce this minimum heterogeneous reactivity. It is stressed that the aforementioned methodology maintains a flame in the reactor, at least for a subrange of the inlet velocities of the non-catalytic case. For very high catalytic reactivities, gas-phase combustion maybe altogether suppressed [26]. Although pure catalytic combustion can be desirable for certain devices, the presence of a flame ensures complete fuel conversion at short channel lengths, which may have otherwise been impossible due to the mass transport limitations of the catalytic pathway.

4. Conclusions

The dynamics of lean premixed hydrogen/air flames were investigated numerically in a 2 mm height channel as a function of the inlet velocity and the wall catalytic reactivity. The latter was controlled by the parameter A_s, the ratio of the catalytically active to the geometrical surface area. It was shown that the rich flame dynamics exhibited in the non-catalytic case, which included non-stationary repetitive ignition/extinction and oscillating flames, can be effectively suppressed by catalytic reactions. The repetitive/ignition extinction was suppressed first for A_s = 0.003, the oscillating flames were eliminated for A_s > 0.01, leaving only the steady closed symmetric and asymmetric flames at higher A_s. Contrary to earlier microscale studies, the present mesoscale simulations indicated that complete restoration of symmetry by increasing A_s in the asymmetric flames was not possible. Finally, the results suggest that a practical way for eliminating undesirable flame dynamics in mesoscale channels is to apply a predetermined catalyst loading on the channel walls.

Acknowledgments

Support has been provided by the Swiss National Foundation via contract 200021-109398 and by Paul Scherrer Institute.

References

[1] A.C. Fernandez-Pello, Proc. Combust. Inst. 29 (2002) 883–899.
[2] J.M. Ahn, C. Eastwood, L. Sitzki, P.D. Ronney, Proc. Combust. Inst. 30 (2005) 2463–2472.
[3] D.G. Norton, E.D. Wetzel, D.G. Vlachos, Ind. Eng. Chem. Res. 43 (2004) 4833–4840.
[4] S. Karagiannidis, J. Mantzaras, G. Jackson, K. Boulouchos, Proc. Combust. Inst. 31 (2007) 3309–3317.
[5] U. Dogwiler, J. Mantzaras, P. Benz, B. Kaeppeli, R. Bombach, A. Arnold, Proc. Combust. Inst. 27 (1998) 2275–2282.
[6] K. Maruta, T. Kataoka, N.I. Kim, S. Minaev, R. Fursenko, Proc. Combust. Inst. 30 (2005) 2429–2436.
[7] F. Richecoeur, D.C. Kyritsis, Proc. Combust. Inst. 30 (2005) 2419–2427.
[8] G. Pizza, C.E. Frouzakis, J. Mantzaras, A.G. Tomboulides, K. Boulouchos, Combust. Flame 152 (2008) 433–450.

[9] G. Pizza, C.E. Frouzakis, J. Mantzaras, A.G. Tomboulides, K. Boulouchos, Combust. Flame 155 (2008) 2–20.
[10] V.N. Kurdyumov, E. Fernandez-Tarrazo, J.-M. Truffaut, J. Quinard, A. Wangher, G. Searby, Proc. Combust. Inst. 31 (2007) 1275–1282.
[11] V.N. Kurdyumov, J.-M. Truffaut, J. Quinard, A. Wangher, G. Searby, Combust. Sci. Technol. 180 (2008) 731–742.
[12] G. Pizza, J. Mantzaras, C.E. Frouzakis, A.G. Tomboulides, K. Boulouchos, Proc. Combust. Inst. 32 (2009) 3051–3058.
[13] M.E. Coltrin, R.J. Kee, F.M. Rupley, Surface CHEMKIN: a Fortran package for analyzing heterogeneous chemical kinetics at the solid surface–gas phase interface, Report No. SAND90-8003C, Sandia National Laboratories, 1996.
[14] A. Schneider, J. Mantzaras, S. Eriksson, Combust. Sci. Technol. 180 (2008) 89–126.
[15] S. Eriksson, A. Schneider, J. Mantzaras, M. Wolf, S. Järås, Chem. Eng. Sci. 62 (2007) 3991–4011.
[16] T.J. Kim, R.A. Yetter, F.L. Dryer, Proc. Combust. Inst. 25 (1994) 759–766.
[17] O. Deutschmann, R. Schmidt, F. Behrendt, J. Warnatz, Proc. Combust. Inst. 26 (1996) 1747–1754.
[18] R.J. Kee, G. Dixon-Lewis, J. Warnatz, M.E. Coltrin, J.A. Miller, A Fortran computer code package for the evaluation of gas-phase multicomponent transport properties, Report No. SAND86-8246, Sandia National Laboratories, 1996.
[19] R.J. Kee, F.M. Rupley, J.A. Miller, Chemkin II: a Fortran chemical kinetics package for the analysis of gas-phase chemical kinetics, Report No. SAND89-8009B, Sandia National Laboratories, 1996.
[20] M.O. Deville, P.F. Fischer, E.H. Mund, High-Order Methods for Incompressible Fluid Flow, Cambridge University Press, New York, 2002.
[21] A.G. Tomboulides, J. Lee, S.A. Orszag, J. Sci. Comput. 12 (1997) 139–167.
[22] G.D. Byrne, A.C. Hindmarsh, Int. J. High Perform. Comput. Appl. 13 (1999) 354–365.
[23] T. Poinsot, D. Veynante, Theoretical and Numerical Combustion, Edwards, 2005, p. 56.
[24] F.M. Rupley, R.J. Kee, J.A. Miller, Premix: a Fortran program for modeling steady laminar one-dimensional premixed flames, Report No. SAND85-8240, Sandia National Laboratories, 1995.
[25] A. Cavaliere, M. de Joannon, Prog. Energy Combust. Sci. 30 (2004) 329–366.
[26] J. Mantzaras, C. Appel, Combust. Flame 130 (2002) 336–351.